Materials Today • Volume 55 • May 2022 RESEARCH

RESEARCH: Original Research

Electrochemical swelling induced high material utilization of porous polymers in magnesium electrolytes

Xiaojun Wang [1,2,3,†], Hui Dong [2,3,†], Alae Eddine Lakraychi [2,3], Ye Zhang [2,3], Xu Yang [2], Hongzhi Zheng [2,3], Xinpeng Han [2,3], Xiaonan Shan [2], Chuanxin He [1,*], Yan Yao [2,3,*]

[1] Shenzhen Key Laboratory for Functional Polymer, College of Chemistry and Environmental Engineering, Shenzhen University, Shenzhen, Guangdong 518060, China
[2] Department of Electrical and Computer Engineering, University of Houston, Houston, TX 77204 USA
[3] Texas Center for Superconductivity at the University of Houston (TcSUH), Houston, TX 77204, USA

Magnesium rechargeable batteries are promising candidates for large-scale energy storage due to their - high safety, low material cost, and earthabundant materials. Many redox-active polymers have recently been reported to show excellent cycling stability with decent Mg-storage performance. However, compared to their Li counterparts, these polymers exhibit lower Mg-storage capacity, resulting in a low ratio of materials utilization (η_{Mg}/η_{Li}) for the same polymer in two electrolyte systems (i.e., Mg vs. Li electrolytes). Herein, we present a sulfur-linked porous polymer, poly(hexaazatrinaphthalene sulfide) (PSHATN), which sets a record for material utilization of 98% among all polymer electrodes and delivers a reversible capacity of 196 mAh g^{-1} in Mg electrolytes. Based on electrochemical impedance spectroscopy and operando optical microscopy, we discover a strong correlation between specific capacity and degree of electrochemical swelling of polymers in both electrolytes. Importantly, the high ratio (η_{Mg}/η_{Li}) of PSHATN is ascribed to sufficient electrochemical swelling due to its large pore volume and flexible polymer nature, in contrast to linear polymers and rigid covalent organic frameworks that swell less effectively. This work highlights the critical need for polymer swelling in promoting ion transport in redox polymers for high material utilization and offers important polymer structural design insights for multivalent ion-based energy storage.

Keywords: Electrochemical swelling; Magnesium rechargeable batteries; Porous polymers; Operando optical microscopy; Polymer–electrolyte interaction

Introduction

The rapid deployment of renewable energy sources such as photovoltaic, wind, and tidal energy calls for next-generation batteries that are safe, high energy, high power, and low cost [1,2]. Rechargeable magnesium batteries are considered among the top candidates for this purpose, owing to their resource abundance, high volumetric capacity (3833 mAh cm^{-3}), and dendrite-free stripping/plating behavior of Mg metal anode [3–7]. However, magnesium batteries utilize divalent Mg^{2+} as charge carriers, which holds twice the amount of charge compared to Li^{+} while having the same ionic radius [8]. This results in a high energy barrier for ion dissociation from electrolyte and sluggish solid-state ion diffusion in insertion host materials at room temperature [5,7]. Whereas weakly-coordinating electrolytes are efficient in ion dissociation [9–14], finding suitable

* Corresponding authors.
E-mail addresses: He, C. (hecx@szu.edu.cn), Yao, Y. (yyao4@uh.edu).
† These authors contributed equally.

1369-7021/© 2022 Elsevier Ltd. All rights reserved. https://doi.org/10.1016/j.mattod.2022.04.010

high-performance cathode materials remains a major challenge toward practical applications of magnesium batteries.

At present, various cathode materials have been explored and evaluated according to their Mg-storage mechanisms [15,16,17]. Intercalation and conversion chemistries are both promising research directions owing to the improved Mg^{2+} insertion kinetics for the former [18–25] and the conversion mechanism bypassing the sluggish ion diffusion for the latter [26–30]. However, state-of-the-art intercalation cathodes, mainly sulfides, still do not fulfil the magnesium cathode requirement due to low specific energy at room temperature [19,20] whereas high-capacity conversion cathodes remain hampered by the high dissolution of the intermediate polysulfides that lead to rapid capacity decay [26,27]. Recently, organic battery electrode materials (OBEMs) have emerged as environmentally friendly, low-cost, transition metal-free electrode materials for electrochemical storage [31–34]. To date, a plethora of promising OBEMs have demonstrated encouraging electrochemical performances in many battery chemistries [35], thanks to their unique charge compensation redox mechanism, flexible molecular design, and insensitivity to the intercalation cation. Pyrene-4,5,9,10-tetraone (PTO) is the best example to illustrate this point [36], with excellent electrochemical performance being demonstrated for mono- [37,38] and multivalent [39,40] metal-storage in aqueous [41] or non-aqueous and even solid-state electrolytes [42–44]. Recently, our group has reported a breakthrough in magnesium batteries using PTO as the cathode material coupled with a weakly coordinating boron cluster-based electrolyte [40]. Thanks to the heterogeneous enolization redox mechanism, an unprecedented specific power (30.4 kW kg^{-1}) was delivered and a high degree of magnesiation was reached. However, dissolution of discharged species in the electrolyte leads to capacity fade upon cycling, and a graphene-oxide modified separator is required to improve the cycling performance.

Redox polymers are known to be capable of overcoming the solubility issue [45,46]. Many groups have reported various polymers showing high cycling stabilities with decent Mg-storage performances at room temperature [47,48]. However, most polymers exhibit significantly lower material utilization in Mg electrolytes (η_{Mg}) compared to their utilization in Li electrolytes (η_{Li}) (Table S1). To quantify this electrolyte effect on materials utilization for the same redox polymer, we consider the ratio of materials utilization (η_{Mg}/η_{Li}) in two representative electrolytes systems (e.g., Mg vs. Li electrolytes). Fig. 1a summarizes η_{Mg}/η_{Li} for various redox polymers reported. Linear polymers (e.g. PAQS [48–50], P14AQ [47,48,51], PNDIE) show η_{Mg}/η_{Li} in the range of 41 ∼ 52% while COF-based rigid porous polymers (COF-BPOE [52,53], PHATN [54]) show higher η_{Mg}/η_{Li} approaching 71%. In this work, we present a flexible and amorphous porous polymer, poly(hexaazatrinaphthalene sulfide) (PSHATN), with a record η_{Mg}/η_{Li} value of 98% at a high capacity of 196 mAh g^{-1} (Fig. 1a). An unconjugated sulfur linker is adopted to enable polymer conformations with greater flexibility, whereas the porous nature facilitates efficient electrolyte uptake. For comparison, two linear polymers poly[N,N′-(ethane-1,2-diyl)-1,4,5,8-naphthalenetetracarboxyimide] (PNDIE) and poly(anthraquinonyl sul-

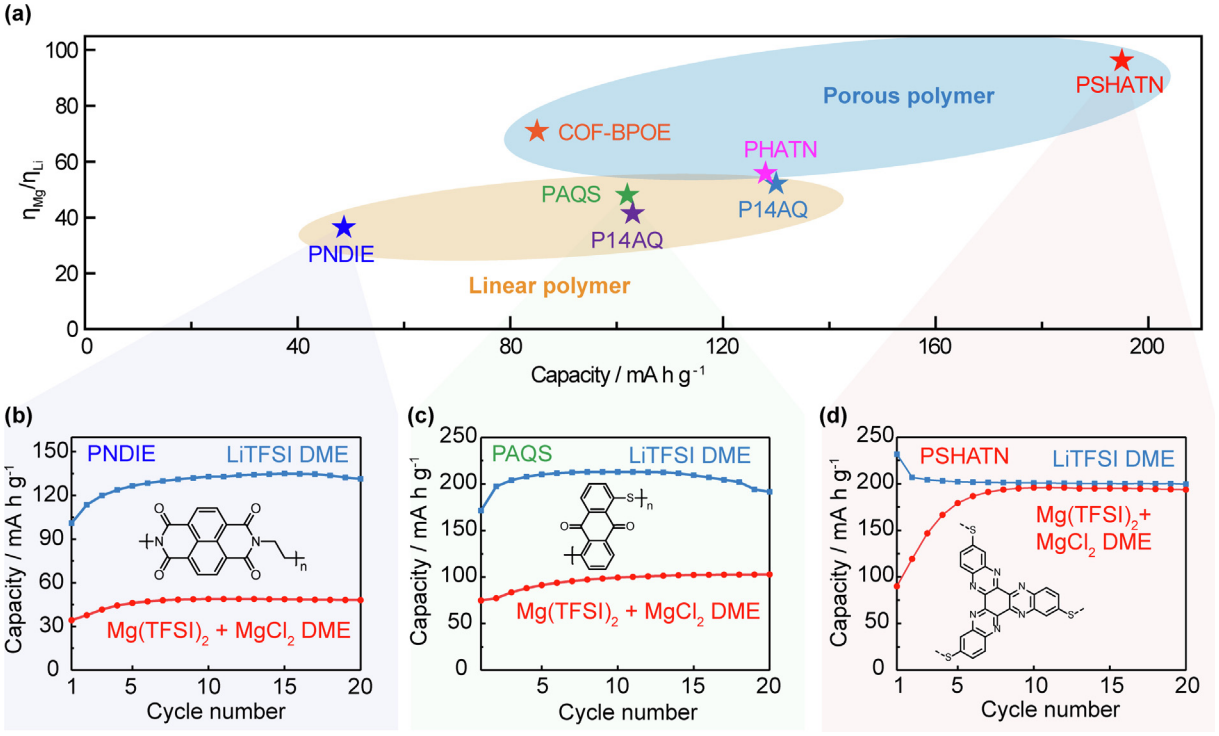

FIGURE 1

Porous redox polymers show a higher ratio of material utilization (η_{Mg}/η_{Li}) than linear redox polymers. (a) Comparing previously reported polymer materials and PSHATN in terms of the ratio of material utilization. (b–d) Electrochemical performance of (b) PNDIE, (c) PAQS, and (d) PSHATN in Mg electrolyte (0.25 M $Mg(TFSI)_2$ + 0.5 M $MgCl_2$ in DME) vs. Li electrolyte (0.5 M LiTFSI in DME) at 0.5C. For PAQS, 1C = 225 mAh g^{-1}; for PNDIE, 1C = 183 mAh g^{-1}; for PSHATN polymer, 1C = 374 mAh g^{-1}.

fide) (PAQS) were studied. The PSHATN electrodes show one order of magnitude higher ionic condu higher ionic conductivity than that in PAQS and PNDIE due to the porous structure and sufficient and facile electrochemical swelling.

Results and discussion

Preparation and characterization of PSHATN, PAQS and PNDIE

PSHATN, PAQS, and PNDIE were synthesized and characterized according to the experimental conditions in the supplementary information. Briefly, PSHATN was obtained in a two-step synthesis consisting of a condensation reaction between 4-fluoro-1,2-phenylenediamine and hexaketocyclohexane, followed by a polymerization step using Na_2S; whereas PAQS and PNDIE were produced via polymerization of 1,5-dichloroanthraquinone and 1,4,5,8-naphthalenetetracarboxylic dianhydride, respectively. The formation of the desired polymers was confirmed by Fourier-transform infrared spectroscopy (FTIR) (Fig. S1). N_2 adsorption–desorption isotherm measurements were performed to evaluate the surface area and porosity of the synthesized powders. The total pore volume (P/P_0 = 0.995) and specific surface of PSHATN are 0.3 $cm^3\ g^{-1}$ and 268 $m^2\ g^{-1}$ respectively, notably higher than those for PAQS (0.13 $cm^3\ g^{-1}$, 53 m1 g^{-1}) and PNDIE (0.1 $cm^3\ g^{-1}$, 19 $m^2\ g^{-1}$). The higher specific surface area and pore volume of PSHATN promote electrolyte uptake and efficient swelling [55]. XRD measurement of PSHATN revealed an amorphous structure in the absence of π–π interaction (Fig. S2).

Ratio of material utilization and cycling performance comparison

The three polymers were investigated as cathode materials vs. Li and vs. Mg in Swagelok cells using Li-based and Mg-based electrolytes, respectively. For the sake of comparison, we chose electrolytes with the same solvent and anions except for the cation, namely LiTFSI in dimethoxyethane (DME) and $Mg(TFSI)_2/MgCl_2$ (1:2) in DME. It is worth noting that the complex solvated cations in these solutions are $Li^+(DME)_3$ [56,57] for Li electrolytes and $[Mg_2Cl_2]^{2+}(DME)_4$ [13,58–60] for Mg electrolytes. Multiple studies showed that ion storage takes place in their solvated forms in polymers [61–64], therefore the size of these solvated cationic species should be taken into consideration during the charge storage process. For simplicity, we will mention the storage of Li^+ and $MgCl^+$ instead of $Li^+(DME)_3$ and $[Mg_2Cl_2]^{2+}(DME)_4$ throughout this article.

As expected, the galvanostatic charge/discharge curves for PAQS and PNDIE display an efficient reversible lithiation/delithiation processes at average discharge potentials of 2.15 and 2.33 V vs. Li^+/Li with specific capacities of 172 and 101 mAh g^{-1} in the first cycle, respectively (Fig. S3a and c). However, during the magnesiation/demagnisiation process, lower potentials of 1.52 and 1.54 V vs. Mg^{2+}/Mg and specific capacities of 75 and 34 mAh g^{-1} in the first cycle were observed for PAQS and PNDIE respectively (Fig. S3b and S3d). The difference in redox potentials between Li and Mg half-cells is in accordance with the empirical value of 0.7 V difference between Li and Mg [65]. Interestingly, the electrochemical process for both linear polymers shows slight increases in capacity upon cycling before reaching a maximum value in both Li and Mg half-cells, indicating an activation process that could be attributed to the swelling effect. However, the η_{Mg}/η_{Li} is limited to 48% for PAQS and 36% for PNDIE, which is attributed to the sluggish $MgCl^+$ diffusion and the slow electrolyte uptake due to the low pore volume of both polymers (Fig. 1b and 1c).

The charge/discharge profile of PSHATN shows two distinct plateaus located at ~2.42 and ~1.53 V vs. Li^+/Li, corresponding to a specific capacity of 201 mAh g^{-1} which is maintained over 10 cycles in Li half-cells (Fig. S3e). Surprisingly, in Mg half-cells, the porous polymer reveals a sloping voltage profile in the first cycle, while three distinct plateaus are observed in later cycles (Fig. S3f). This kind of behavior is usually attributed to an activation process, which could be promoted by the swelling process of PSHATN in the electrolyte. Moreover, this activation process is accompanied by a significant increase in capacity from 90 mAh g^{-1} (1st cycle) to 196 mAh g^{-1} (10th cycle). Additionally, the PSHATN/Mg half-cell shows excellent cycling stability after the initial activation process, maintaining a specific capacity of 142 mAh g^{-1} after 500 cycles (Fig. S4), as one of the most stable polymer cathodes in magnesium batteries [48,50,53,54].

Thanks to its porous nature, PSHATN exhibits a higher magnesiation degree and therefore a higher η_{Mg}/η_{Li} of 98% (Fig. 1a and d). This number is not only higher than linear polymers (e.g. 48% for PAQS and 36% for PNDIE) but also higher compared to other COF-based porous polymers, e.g., 71% for COF–BPOE [52,53] and 56% for PHATN [54]. The previously reported COF-based polymers experience a less efficient swelling process originating from their rigid conjugated frameworks, crystalline nature, and strong π−π interaction. In contrast, PSHATN benefits from its flexible, sulfur-linked non-conjugated framework and amorphous nature, which enable the polymer to sufficiently swell in electrolytes. The Li and Mg content in discharged PSHATN electrodes are measured by Inductive Coupled Plasma Emission Spectrometer (ICP) (Table S2). The Mg/Li ratio of 0.92 is consistent with the high η_{Mg}/η_{Li} of 0.98, which confirms the high magnesiation degree. The Mg/Li ratio for discharged electrodes is close to 1, indicating the charge storage in the electrodes is monovalent. Note that the energy-dispersive X-ray results show that $MgCl^+$ can be taken up and released from PSHATN (Fig. S5), which is in line with the Mg/Li ratio and previous reports [47].

The electrochemical activation process of PSHATN

To better understand the electrochemical behavior of PSHATN, electrochemical impedance spectroscopy (EIS) at steady state was performed to assess the activation process of the polymer in both Li and Mg half-cells (Fig. S6). Three-electrode Swagelok cells were used to exclude the influence of the anode. In the Li electrolyte, PSHATN exhibits a large interfacial impedance at the initial state (OCV), which decreases significantly right after the 1st cycle and then increases gradually upon cycling (10 cycles) without affecting the capacity (201 mAh g^{-1}) (Fig. 2a). This rapid drop in the interfacial impedance indicates a facile activation process, which can be explained by the- fast diffusion of smallsized Li ions. In contrast, in the Mg electrolyte, the interfacial impedance decreases progressively after the first cycle, indicating a slow activation process (Fig. 2b). Such a phenomenon could be ascribed to the sluggish diffusion of bulky $MgCl^+$ ions, which improves with electrolyte swelling of the polymer upon

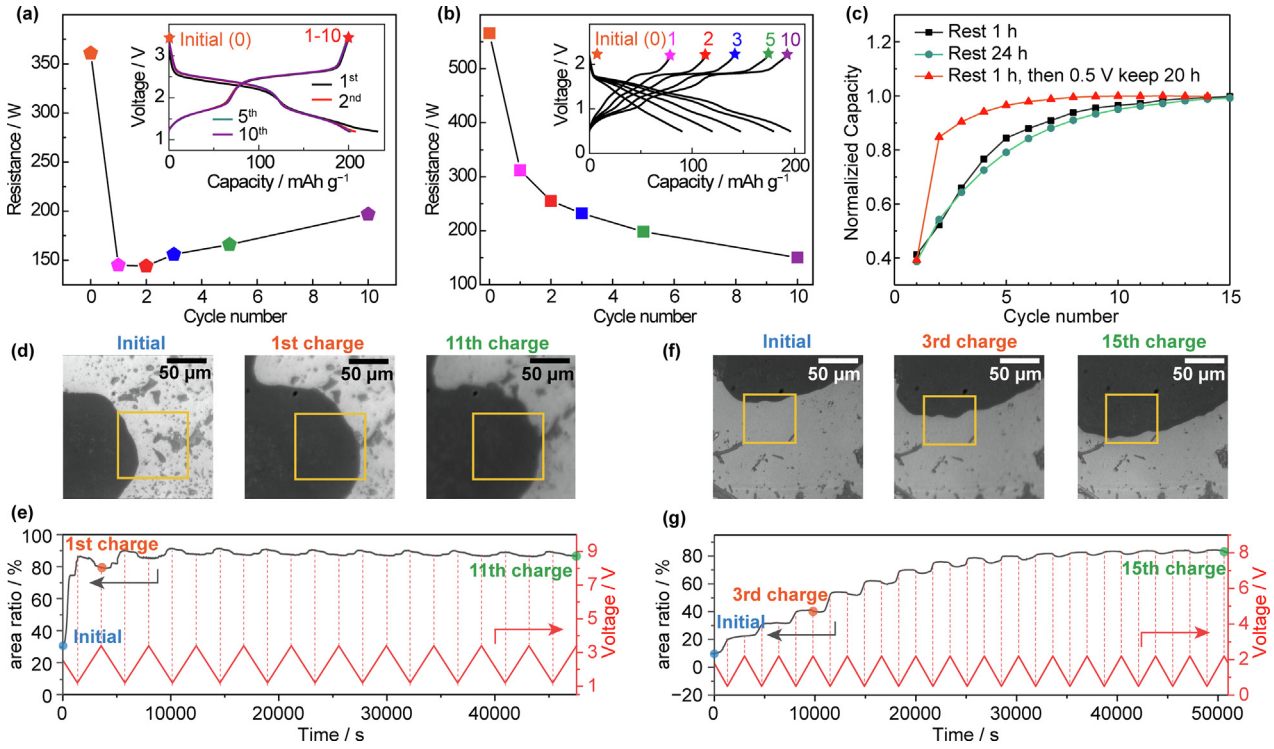

FIGURE 2

The electrochemical activation process and operando optical microscopic imaging. (a-b) Interfacial resistance vs. cycle number plot obtained from electrochemical impedance spectroscopy (EIS) of PSHATN electrodes in (a) Li and (b) Mg electrolyte. The insets show the corresponding galvanostatic charge–discharge voltage profiles of PSHATN at 0.5C (187 mA g^{-1}) for the first 10 cycles. (c) Comparison of the normalized capacity with 1-hour rest, 24-hour rest before discharging, and the one with 1-h rest then 20-h constant voltage hold at 0.5 V after the first constant-current discharge process. (d and f) Optical images of samples collected at various states of charge are shown in (e) and (g). The area ratio % is calculated from the yellow square highlighted in the images. (e and g) Voltage profiles and electrode area ratio (%) of PSHATN electrode in Li and Mg electrolytes during cycle voltammetry measurements at a scan rate of 1 mV s^{-1}.

cycling. Note that the lowest impedance value is attained after the 10th cycle, which corresponds to the highest capacity (196 mAh g^{-1}). In this regard, one would wonder whether the swelling requires an electric field, or whether it is just a matter of time for the polymer to swell in the presence of an electrolyte. To verify this, we held the voltage at the discharge state (0.5 V) for 20 hours, prior to charge/discharge cycling (Fig. S7). This electrochemical holding at the discharge state promotes enhanced swelling of redox polymers at the discharge state. Another cell with a simple rest at OCV (24 h) was also evaluated for comparison. As shown in Fig. 2c, the cell with electrochemical holding at 0.5 V displays a rapid capacity increase after the first cycle, which stabilizes at its maximum value during the subsequent cycles. However, the cell resting at OCV for 24 hours does not facilitate the swelling and still exhibits a progressive capacity increase before reaching the maximum value, as observed for the cell with a rest period of 1 hour (Fig. S3f). Overall, this shows that the activation process of PSHATN electrodes is caused by an electrochemically driven polymer swelling in the electrolyte, which will be discussed in the next section.

Evidence of electrochemical swelling of PSHATN

Although polymer swelling with a plasticizer is a well-known phenomenon in solid (or inggel) polymer electrolytes that are key to enhancing ionic conductivity [55], the effect of swelling on the battery performances of polymer electrodes has not yet been studied. During the redox process, electrolyte uptake and evolution of polymer chains would lead to the increase of pore volumes and facilitate ion transport, while the internal stress of polymer backbones decreases during the redox reaction, potentially leading to increased cycling stability [66].

The discovery of the relationship between the migration of $MgCl^+$ cations into the electrode and the activation process has prompted us to experimentally verify the occurrence of the electrode volume change during cycling. For this purpose, we developed an in-house operando cell for optical imaging. The cell was fitted with a 5 mm observation window in the center of the positive case, in which a transparent ITO glass was placed as a current collector (Fig. S8), and the ITO window was carefully sealed with epoxy. An upright optical microscope was used to image the electrode volume change during the charge/discharge process through the ITO window for both Li and Mg half-cells (see the experimental for details). The operando optical imaging provides a direct observation of morphological evolution of PSHATN electrodes during cycling. In the video of the Li electrolyte (Supplementary video 1), the dark region in the video corresponds to the PSHATN electrode, whereas the bright region corresponds to the glass fiber separator. We observed a significant expansion and contraction of the electrode during the discharge and charge, respectively. To quantify this volume change, we calculated the electrode area ratio in a selected square (highlighted in yellow) in Fig. 2d. The corresponding area ratio during the ini-

tial 11 cycles is presented in Fig. 2e. In the first cycle, the electrode area expanded rapidly from 32.4% to 86.7% during discharge and then shrank to 79.0% after charge. Afterwards, the electrode area ratio increased only slightly and then remained steady during the subsequent cycles. The detailed analysis of the volume expansion and contraction processes of each cycle is shown in Fig. S9a.

In contrast to the Li electrolyte, the volume change of the electrode in Mg electrolyte revealed a different phenomenon (Supplementary video 2 and Fig. 2f). The electrode underwent a continuous volume expansion over cycling, which translates into a gradual increase of the electrode area ratio during the initial 13 cycles (Fig. 2g). Afterwards, the electrode area became stable with relatively small expansion and contraction. This indicates that the swelling process of the polymer in the Mg electrolyte is much slower than in its Li counterpart, which can be highly attributed to the slow kinetics of $MgCl^+$ ions since the same solvent was used for both experiments (e.g., dimethoxyethane, DME). However, once the initial swelling step is completed, the volume variation is as little as 3% during the rest of the cycles, which alleviates the volume expansion and its associated issues upon cycling that are usually encountered for large-capacity cathode materials. Analysis of the expansion and contraction of the electrode for each cycle is shown in Fig. S9b.

The above observation echoes the results obtained from galvanostatic charge/discharge and EIS shown in Fig. 2a and b, demonstrating that the activation process is directly linked to the polymer–electrolyte interaction. The fast swelling process in Li electrolyte enables a fast wettability of the electrode and offers better polymer–electrolyte contact, leading to high capacity from the first cycle, whereas slow swelling in Mg electrolyte facilitates $MgCl^+$ ion diffusion that improves with charge/discharge cycles and leads to a gradual capacity increase to reach the stable capacity after 13 cycles.

Sufficient swelling for a high ratio of material utilization

In order to accelerate the swelling process of PSHATN in Mg electrolytes, we conducted a pre-swelling step of PSHATN electrodes in Li electrolyte before cycling in Mg electrolyte. Fig. 3a illustrates the preparation process. Briefly, the PSHATN electrode was allowed to cycle in Li electrolyte for one cycle to achieve enough swelling. Next, the electrode was extracted at the charge state and washed with DME to fully remove lithium salts, and then reloaded into a Mg cell with a fresh Mg electrolyte for electrochemical characterization. As expected, the PSHATN electrode reaches its maximum capacity at the first cycle, and scales perfectly with the capacities obtained in the Li half-cell and Mg half-cell without pre-cycling (Fig. 3b). The same experiment

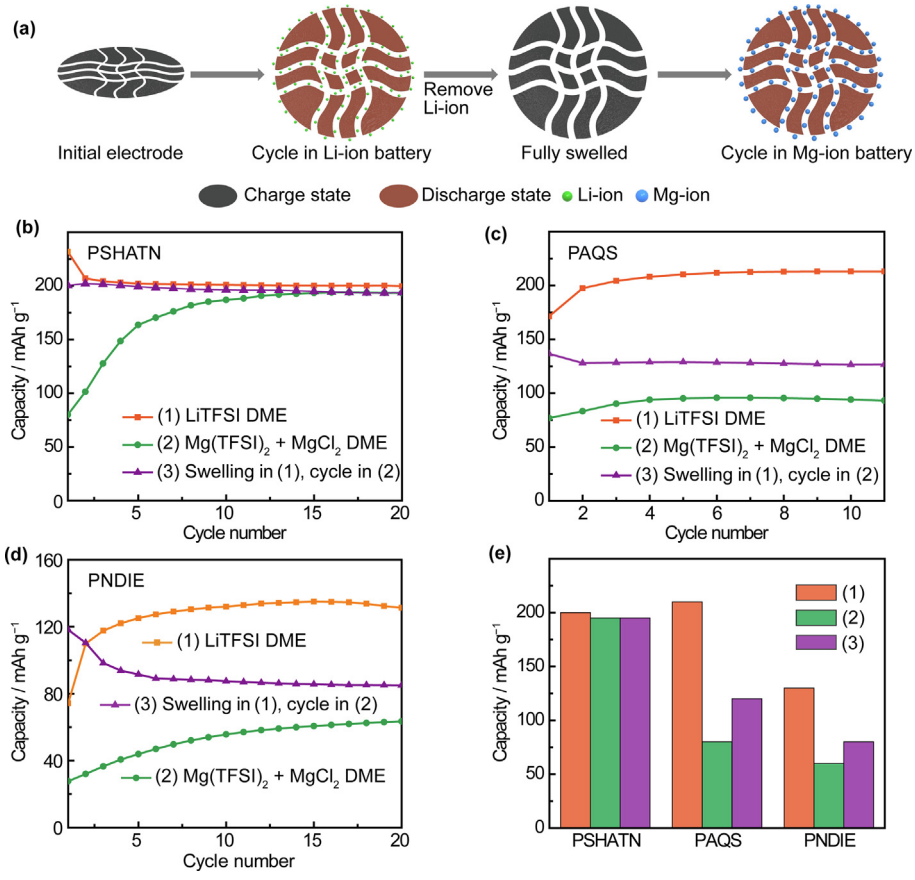

FIGURE 3

Porous polymer (PSHATN) shows a consistently higher ratio of material utilization than linear polymers (PAQS, PNDIE). (a) Schematic of procedure 3: pre-activation in Li electrolytes, followed by cycling in Mg electrolytes. (b–d) PSHATN, PAQS and PNDIE capacity retention profiles in various cycling procedures. (e) Plot of PSHATN, PAQS and PNDIE capacity at the 10th cycle obtained in Li electrolyte (1), Mg electrolyte (2), and Mg electrolyte after the pre-activation in Li electrolyte (3).

was also conducted for PAQS and PNDIE electrodes with 5 cycle (PAQS) and 10 cycle (PNDIE) activation in Li electrolytes to reach a stable capacity. Despite the pre-swelling step increaseing the η_{Mg}/η_{Li} of PAQS and PNIDE electrodes compared to those obtained without pre-cycling (Fig. 3c and d), the capacities in Mg half-cells still can't match those attained in Li half-cells (Fig. 3e). These results confirm that even if lithium ions can enter the PAQS and PNDIE electrodes to assist their electrochemical swelling process, the pore volume inside the PAQS and PNDIE polymers can't support the facile diffusion of $MgCl^+$. Overall, both polymer swelling and larger pore volume benefit higher the η_{Mg}/η_{Li} of PSHATN.

Kinetics of ion transport

As stated above, the redox process plays an important role in the activation process, triggering the swelling of PSHATN while the latter leads to enhanced ion diffusion and thus higher capacity. Since the swelling needs to be assisted with an electrochemical reaction, it seems judicious to correlate the degree of polymer swelling with charge carrier diffusivity. In this vein, cyclic voltammetry (CV) at different scan rates was conducted to study the ion diffusion kinetics for PSHATN as well as PAQS and PNDIE in Li and Mg electrolytes. The redox process for the three polymers, as shown in Fig. 4a, contains a significant portion of surface controlled reaction (*b* value is closer to 1) in Li electrolyte [67], implying a fast Li^+ ion diffusion into the electrode. On the other hand, as shown in Fig. 4b and Fig. S10, the redox process in Mg electrolyte is characterized by a diffusion-controlled reaction (*b* value is closer to 0.5) due to the larger size of $MgCl^+$ ions [67]. Because the polymers swell, the charge carrier moves faster for Li^+ and slower for $MgCl^+$, which means that the swelling of the polymers affects how quickly the charge carrier moves.

To study the relationship between ion transport kinetics and η_{Mg}/η_{Li}, we performed galvanostatic intermittent titration technique (GITT) to determine the diffusion rate of $MgCl^+$ ions as a function of state-of-discharge for the three polymer electrodes studied here. All the electrodes were tested after completing the activation process and attained stable capacity. The GITT curves reveal a relatively low polarization for the three polymers and confirm the existence of three different plateaus for PSHATN (Fig. 4c, PAQS, and PNDIE in Fig. S11). The diffusion coefficient for each polymer is calculated from the corresponding GITT curve and plotted as a function of capacity (Fig. 4d and Fig. S12). For PSHATN, the diffusion coefficient rises stepwise during the discharge of PSHATN and decreases stepwise during the charging process. This observation aligns to the electrochemo-mechanical "breathing" phenomenon observed in the operando optical microscopy.

Similar trends were also observed for PAQS and PNDIE, as the diffusion coefficient tends to increase and decrease during the discharge charge processes (Fig. S12), a common phenomenon for the three polymers. The comparison of the three polymers reveals PSHATN has a diffusion coefficient 10^{-9} cm^2 s^{-2}, an order of magnitude higher than that for PAQS and PNDIE (Fig. 4d). Finally, the fast diffusion of $MgCl^+$ into PSHATN electrode stems

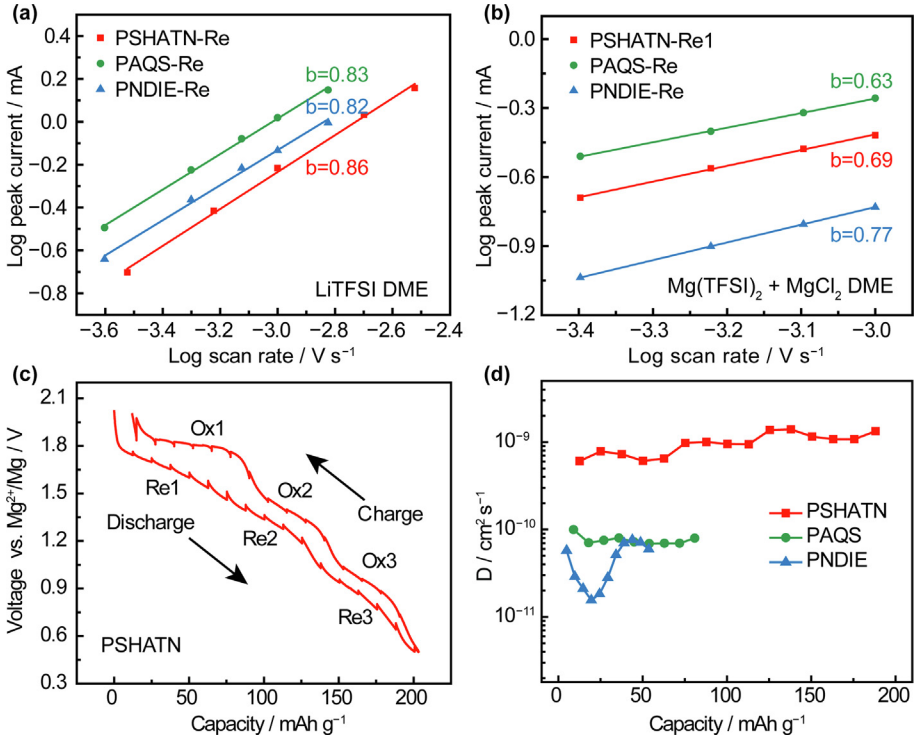

FIGURE 4

Ion transport in porous polymers (PSHATN) is faster than in linear polymers (PAQS, PNDIE). (a and b) Peak current vs. scan rate of PSHATN, PAQS, and PNDIE and PSHATN in the Li electrolyte and Mg electrolyte. (c) Galvanostatic intermittent titration technique (GITT) profiles of the PSHATN electrode in the Mg electrolyte. (d) Diffusion coefficients were extracted from the GITT results.

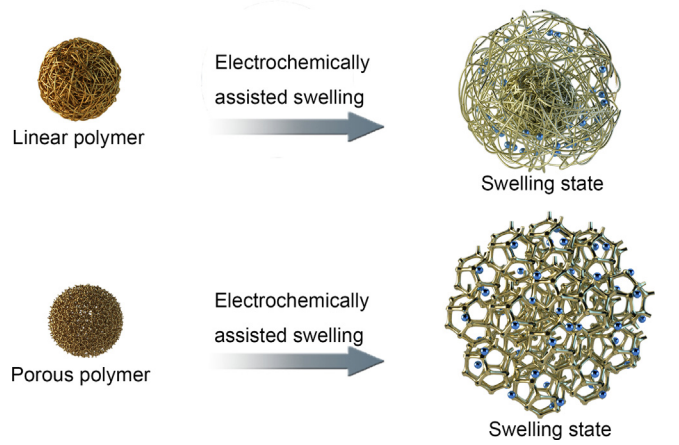

SCHEME 1

Schematic comparison of electrochemically assisted swelling of linear and porous redox polymers. Insufficient swelling of linear polymers in electrolytes leads to partial utilization of active materials. In contrast, sufficient swelling of porous polymers provides higher utilization.

from its high swelling ability and inherent large pore volume, which leads to high a η_{Mg}/η_{Li}. We expect that this ability can be extended to other multi-valent charge carriers such as Ca^{2+} and Zn^{2+}, which will be reported in future studies.

Conclusion

In this work, we have investigated the electrochemical performances of three polymers—PSHATN, PAQS, and PNDIE—in Li and Mg electrolytes. As illustrated in Scheme 1, we demonstrate that flexible porous polymers (e.g. PSHATN) with an inherent large pore volume are able to swell efficiently with a high ratio of material utilization (η_{Mg}/η_{Li} ~98%) as confirmed with a high diffusion coefficient of 10^{-9} cm^2 s^{-1}. On the other hand, linear polymers (e.g. PAQS and PNDIE) with smaller pore volumes couldn't swell completely, resulting in limited $MgCl^+$ diffusion and therefore lower η_{Mg}/η_{Li}. The degree of polymer swelling is dictated by the polymer–electrolyte interaction at various states of charge. The evolution of the polymer microstructure by X-ray or neutron scattering during the redox process requires careful investigations in the future, and modeling of the relationship between the solvated electrolyte species and porous polymer structures at the molecular level is required for quantitative understanding. Nonetheless, the flexible porous polymer cathode and polymer–electrolyte interaction shown here will help to advance the development of redox polymers for multivalent metal ion-based energy storage.

Methods

Synthesis

The synthetic procedures of the PSHATN, PAQS, and PNDIE and their characterization are thoroughly reported in the supplementary information.

Electrode preparation

Redox-active polymers (PSHATN or PAQS, PNDIE), Ketjenblack carbon (KB), and polytetrafluoroethylene (PTFE) binder were hand-mixed in a 6:3:1 mass ratio with the aid of ethanol and pressed to form freestanding electrodes with an areal mass loading of ~5 mg cm^{-2}. All electrodes were dried at 80 °C under vacuum for 24 h prior to use.

Electrolyte preparation

Electrolytes were prepared inside an Ar-filled glove box (M-Braun Co., <0.5 ppm of water and oxygen). To prepare 0.5 M LiTFSI in DME, LiTFSI (Millipore Sigma, 99.95%) was dried at 150 °C under vacuum for 12 h and DME solvent was dried using molecular sieves over 24 h. 0.287 g of dry LiTFSI powder was dissolved in 2 ml dry DME to obtain the electrolyte. To prepare 0.25 M $Mg(TFSI)_2$ and 0.5 M $MgCl_2$ in DME electrolyte, 0.73 g $Mg(TFSI)_2$ powder (Solvionic, 99.5%) was added to a suspension of $MgCl_2$ (Alfa Aesar, 99.999%, 0.24 g in 5 ml dry DME). The mixture was stirred at 70 °C for 6 h in a sand bath and then cooled down to room temperature to afford a clear solution.

Electrochemical measurements

All experiments were conducted at 25 °C, using a potentiostat (VMP-3, Bio-Logic Co., Claix, France) or a battery tester (LAND CT-2001A). All cells were assembled and tested in an argon-filled glovebox (M-Braun Co., Garching, Germany, <0.5 ppm of water and oxygen). Cells were rest for 1 hour after assembling to allow polymer electrode swelling in the electrolyte unless otherwise indicated. For a Li/PSHATN (or Li/PAQS, Li/PNDIE) full cell, a lithium foil was used as an anode, and a PSHATN (or PAQS, PNDIE) electrode was used as a cathode. 0.5 M LiTFSI in dry DME was used as electrolyte. Two-electrode Swagelok cells (molybdenum rods as the current collectors to avoid corrosion issues) and glass fiber separators were used. For electrochemical impedance spectroscopy (EIS) measurement, to focus on the cathode electrochemical reaction and avoid the influence of anode reaction, three-electrode Swagelok cells (molybdenum rods as the current collectors to avoid corrosion issues) were used with lithium foils as counter and reference electrode, respectively. For an Mg/PSHATN (or Mg/PAQS, Mg/PNDIE) full cell, an Mg foil (50 μm thick, 99.95%, GalliumSource, LLC, Scotts Valley, CA) was used as an anode, and a PSHATN (or PAQS, PNDIE) electrode was used as a cathode. To focus on the polymer cathode electrochemical reaction and avoid the influence of anode reaction, three-electrode Swagelok cells (molybdenum rods as the current collectors to avoid corrosion issues, Mg foil as counter electrode and reference electrode) and glass fiber separators were used for all battery cycling, electrochemical impedance spectroscopy (EIS) measurement, cyclic voltammetry (CV) and the galvanostatic intermittent titration technique (GITT) measurement. 0.25 M $Mg(TFSI)_2$ and 0.5 M $MgCl_2$ in DME was used as electrolyte. To measure EIS at a steady state, the cells were rested for at least 5 min before the measurement.

Operando optical microscopic imaging

Li/PSHATN and Mg/PSHATN full cells were established in coin cells. The battery model is shown in Fig. S8. ITO glass is used as a transparent current collector. Stainless steel foil was used to conduct electrons between ITO and the positive case. The battery was assembled and tested in an argon-filled glovebox. A microscope inside the glovebox is used to observe electrode changs. Images were recorded with a CCD camera (FLIR Blackfly

S USB 3, 720 × 540 pixels) on an Olympus BX60 upright microscope. Synchronous cyclic voltammetry was applied to the coin cell. Image J software was used to transfer operando pictures to videos and analyze the electrode area according to average light intensity in the selected region. The average light intensity of the bright region of the glass fiber separator is defined as zero electrode area, and the average light intensity of the dark region of the electrode was defined as 100% electrode area. There is a linear relationship between the average light intensity and the electrode area in the selected region. The result is real-time corrected by the light intensity of glass fiber and electrode in the same picture.

CRediT authorship contribution statement

Xiaojun Wang: Conceptualization, Formal analysis, Methodology, Investigation, Validation, Visualization. **Hui Dong:** Conceptualization, Methodology, Investigation, Validation, Writing – review & editing. **Alae Eddine Lakraychi:** Methodology, Writing – review & editing. **Ye Zhang:** Methodology, Validation, Writing – review & editing. **Xu Yang:** Methodology. **Hongzhi Zheng:** Methodology. **Xinpeng Han:** Methodology. **Xiaonan Shan:** Methodology, Software. **Chuanxin He:** Conceptualization, Funding acquisition, Supervision, Writing – review & editing. **Yan Yao:** Conceptualization, Funding acquisition, Supervision, Writing – review & editing, Project administration.

Declaration of Competing Interest

The authors declare that they have no known competing financial interests or personal relationships that could have appeared to influence the work reported in this paper.

Acknowledgements

C.H. and X.W. acknowledge the funding support from the National Natural Science Foundation of China (21975162) and Shenzhen Science and Technology Program (Grant No. JCYJ20200109105803806 and JCYJ20180507182057026). Y.Y. acknowledges the Cullen College of Engineering Professorship from the University of Houston.

Data availability

The authors declare that the main data supporting the findings of this study are available within the article and its Supplementary Information files. All other relevant data are available from the corresponding author upon reasonable request.

Appendix A. Supplementary data

Supplementary data to this article can be found online at https://doi.org/10.1016/j.mattod.2022.04.010.

References

[1] J. Muldoon, C.B. Bucur, T. Gregory, Chem. Rev. 114 (2014) 11683–11720.
[2] J.W. Choi, D. Aurbach, Nat. Rev. Mater. 1 (2016) 16013.
[3] Y. Liang et al., Nat. Energy 5 (2020) 646–656.
[4] H.D. Yoo et al., Energy Environ. Sci. 6 (2013) 2265–2279.
[5] R. Mohtadi, F. Mizuno, Beilstein J. Nanotechnol. 5 (2014) 1291–1311.
[6] P. Saha et al., Prog. Mater. Sci. 66 (2014) 1–86.
[7] R. Attias et al., Joule 3 (2019) 27–52.
[8] C.B. Bucur et al., J. Phys. Chem. Lett. 6 (2015) 3578–3591.
[9] W. Ren et al., ACS Energy Lett. 6 (2021) 3212–3220.
[10] Y. Shao et al., Nano Energy 12 (2015) 750–759.
[11] O. Tutusaus et al., Angew. Chem. Int. Ed. 54 (2015) 7900–7904.
[12] Z. Zhao-Karger et al., J. Mater. Chem. A 5 (2017) 10815–10820.
[13] N.N. Rajput et al., Top. Curr. Chem. 376 (2018) 19.
[14] J. Luo et al., Angew. Chem. Int. Ed. 58 (2019) 6967–6971.
[15] M. Mao et al., Chem. Soc. Rev. 47 (2018) 8804–8841.
[16] P. Canepa et al., Chem. Rev. 117 (2017) 4287–4341.
[17] Y. Li et al., Nano Energy 27 (2016) 8–16.
[18] Y. Shen et al., Adv. Mater. 32 (2020) e1905524.
[19] H.D. Yoo et al., Nat. Commun. 8 (2017) 339.
[20] Y. Liang et al., Nano Lett. 15 (2015) 2194–2202.
[21] L. Zhou et al., Adv. Mater. 30 (2018) e1801984.
[22] D. Aurbach et al., Nature 407 (2000) 724–727.
[23] L.F. Wan et al., Chem. Mater. 27 (2015) 5932–5940.
[24] X. Sun et al., Energy Environ. Sci. 9 (2016) 2273–2277.
[25] Z. Li et al., Nat. Commun. 9 (2018) 5115.
[26] P. Wang, M.R. Buchmeiser, Adv. Funct. Mater. 29 (2019) 1905248.
[27] L. Kong et al., Energy Environ. Mater. 1 (2018) 100–112.
[28] T. Gao et al., Angew. Chem. Int. Ed. 56 (2017) 13526–13530.
[29] Z. Zhao-Karger et al., Adv. Energy Mater. 5 (2015) 1401155.
[30] A. Du et al., Energy Environ. Sci. 10 (2017) 2616–2625.
[31] B. Häupler, A. Wild, U.S. Schubert, Adv. Energy Mater. 5 (2015) 1402034.
[32] Y. Wu et al., Adv. Energy Mater. 7 (2017) 1700278.
[33] S. Lee et al., Adv. Mater. 30 (2018) e1704682.
[34] Y. Lu et al., Chem 4 (2018) 2786–2813.
[35] P. Poizot et al., Chem. Rev. 120 (2020) 6490–6557.
[36] H. Cui et al., ChemElectroChem 8 (2020) 352–359.
[37] Z. Guo et al., Nat. Commun. 11 (2020) 959.
[38] Y.L. Liang, P. Zhang, J. Chen, Chem. Sci. 4 (2013) 1330–1337.
[39] Z. Guo et al., Angew. Chem. Int. Ed. 57 (2018) 11737–11741.
[40] H. Dong et al., Nat. Energy 5 (2020) 1043–1050.
[41] Y. Liang et al., Nat. Mater. 16 (2017) 841–848.
[42] F. Hao et al., ACS Energy Lett. 6 (2020) 201–207.
[43] F. Hao et al., Joule 3 (2019) 1349–1359.
[44] J. Zhang et al., Joule 5 (2021) 1845–1859.
[45] Z.P. Song, H.S. Zhou, Energy Environ. Sci. 6 (2013) 2280–2301.
[46] M. Tang et al., Chin. Chem. Lett. 29 (2018) 232–244.
[47] H. Dong et al., Joule 3 (2019) 782–793.
[48] B. Pan et al., Adv. Energy Mater. 6 (2016) 1600140.
[49] Z. Song, H. Zhan, Y. Zhou, Chem. Commun. (2009) 448–450.
[50] J. Bitenc et al., ChemSusChem 8 (2015) 4128–4132.
[51] Z. Song et al., Angew. Chem. Int. Ed. 54 (2015) 13947–13951.
[52] K. Sakaushi et al., Nat. Commun. 4 (2013) 1485.
[53] R. Sun et al., Nano Lett. 20 (2020) 3880–3888.
[54] M. Mao et al., Angew. Chem. Int. Ed. 58 (2019) 17820–17826.
[55] G. Foran et al., iScience 23 (2020) 101597.
[56] X. Chen et al., Fundam. Res. 1 (2021) 393–398.
[57] K. Xu, A. Von Cresce, ECS Trans. 41 (2012) 187–193.
[58] M. Salama et al., J. Phys. Chem. C 121 (2017) 24909–24918.
[59] N.N. Rajput et al., J. Am. Chem. Soc. 137 (2015) 3411–3420.
[60] N. Sa et al., RSC Adv. 6 (2016) 113663–113670.
[61] G. Inzelt, J. Bácskai, J. Electroanal. Chem. Interfacial Electrochem. 308 (1991) 255–267.
[62] G. Inzelt, J. Bácskai, Electrochim. Acta 37 (1992) 647–654.
[63] X. Fan et al., Angew. Chem. Int. Ed. 57 (2018) 7146–7150.
[64] T. Ma et al., Cell Rep. Phys. Sci. 2 (2021) 100414.
[65] T. Ichitsubo et al., J. Mater. Chem. A 2 (2014) 14858–14866.
[66] H. Wang et al., J. Mater. Chem. A 8 (2020) 11906–11911.
[67] T. Kim et al., J. Electrochem. Sci. Technol. 11 (2020) 14–25.